



ISSN: 0975-833X

Available online at <http://www.journalcra.com>

INTERNATIONAL JOURNAL  
OF CURRENT RESEARCH

International Journal of Current Research  
Vol. 11, Issue, 09, pp.7133-7136, September, 2019

DOI: <https://doi.org/10.24941/ijcr.36566.09.2019>

## RESEARCH ARTICLE

### NI<sub>0.9</sub>CO<sub>2.1</sub>O<sub>4</sub> MIXED VALENCE OXIDE NANOPARTICLES COMPOSITE ELECTRODE CATALYSTS FOR OXYGEN REDUCTION IN ALKALINE SOLUTIONS

<sup>1</sup>Mamadou Guèye, <sup>1,\*</sup>Makhtar Guène, <sup>2</sup>Abdou Aziz Diagne and <sup>1</sup>Papa Charles Harris Mandiamy

<sup>1</sup>Laboratoire de Chimie Physique Organique et d'Analyse Environnementale, Département de Chimie, Faculté des Sciences et Techniques, Université Cheikh Anta Diop, Dakar, Sénégal

<sup>2</sup>Département de chimie, UFR SATIC, Université Alioune Diop, Bambey, Sénégal

#### ARTICLE INFO

##### Article History:

Received 20<sup>th</sup> June, 2019

Received in revised form

11<sup>th</sup> July, 2019

Accepted 16<sup>th</sup> August, 2019

Published online 30<sup>th</sup> September, 2019

##### Key Words:

Nickel Cobalt Mixed Oxide, Nanoparticles, impedance Spectroscopy, Electrode Catalysts, Spinel, cyclic voltammetry, Specific surface Area, XPS, Warburg Impedance.

#### ABSTRACT

Nickel cobalt mixed valence oxide nanoparticles composite Ni<sub>0.9</sub>Co<sub>2.1</sub>O<sub>4</sub> was prepared by sol-gel method via propionic acid. The cell parameter and the average crystallite size of the Ni<sub>0.9</sub>Co<sub>2.1</sub>O<sub>4</sub> composite are 8.102 Å and 49.57 nm, respectively. The composition and spinel type structure of the binary mixed oxide were characterized by X-ray photoelectron spectroscopy (XPS) combined with cyclic voltammetry (CV). It was found that the as-synthesized composite has a mixed spinel structure. Cyclic voltammetry, electrochemical impedance spectroscopy (EIS) and chronopotentiometry measurements were performed to investigate the electrochemical properties of the composite. The results indicate that Ni<sub>0.9</sub>Co<sub>2.1</sub>O<sub>4</sub> oxide composite offer high electrical reactivity, good stability in alkaline media, and that increasing the polarization potential leads to the decrease in catalytic performance.

Copyright © 2019, Mamadou Guèye et al. This is an open access article distributed under the Creative Commons Attribution License, which permits unrestricted use, distribution, and reproduction in any medium, provided the original work is properly cited.

Citation: Mamadou Guèye, Makhtar Guène, Abdou Aziz Diagne and Papa Charles Harris Mandiamy. 2019. "Ni<sub>0.9</sub>Co<sub>2.1</sub>O<sub>4</sub> mixed valence oxide nanoparticles composite electrode catalysts for oxygen reduction in alkaline solutions. voltammograms", *International Journal of Current Research*, 11, (09), 7133-7136.

## INTRODUCTION

Surface properties are ones of the most important catalysts physical properties. This is due to the fact that the performance of the catalysts is intimately related to the surface parameters. Catalytic surfaces are characterized according to their physical properties and actual performance as a catalyst. The oxides of transition metals, particularly the spinel type oxides (Trasatti, 1994), represent an important class of polyvalent materials for electrocatalysis. As mixed valence oxides, they allow to study the contribution of solid state chemistry to electro catalytic reactivity. These compounds with different physical, physicochemical and interfacial properties, interesting in electrocatalysis are easily obtained and are suitable as anodes or cathodes in electrochemical systems. Spinel oxides with mixed valence may have electrical conductivity or semi-conductivity allowing their direct use as electrode materials or in electronic transfers taking place with relatively low activation energies between cations of different valences by hopping processes (Rios, 1998).

##### \*Corresponding author: Makhtar Guène,

Laboratoire de Chimie Physique Organique et d'Analyse Environnementale, Département de Chimie, Faculté des Sciences et Techniques, Université Cheikh Anta Diop, Dakar, Sénégal.

Their specific surface areas are rather small, especially when obtained at high temperature by ceramic or dry salts decomposition methods. They may have higher specific surface areas when they are obtained at lower temperatures by certain synthesis routes. The electrocatalytic behavior of cobalt-and nickel-based spinel mixed oxides for oxygen reactions (i.e evolution and reduction), depends on oxides composition, thermal decomposition temperatures, solvent and precursors concentration, etc (Hu, 1997; Boggio, 1987; de Chialvo, 1993; Veggetti, 1992). In the present work, we have investigated the electrochemical properties of nickel cobaltite Ni<sub>0.9</sub>Co<sub>2.1</sub>O<sub>4</sub>. Cyclic voltammetry, electrochemical impedance spectroscopy, chronopotentiometry were performed in order to investigate the stability and performance of this electrocatalyst. XRD and BET analysis have been used to examine the structure and specific surface area of the catalyst.

**Experimental:** Ni<sub>0.9</sub>Co<sub>2.1</sub>O<sub>4</sub> spinel oxide was prepared by sol gel technic using Co (NO<sub>3</sub>)<sub>2</sub>.6H<sub>2</sub>O, Ni(NO<sub>3</sub>)<sub>2</sub>.6H<sub>2</sub>O and commercial propionic acid as raw materials. Details of preparation are given elsewhere (Mamadou Guèye, 2016). The XRD patterns of the samples were recorded at 25 °C in Siemens D500 diffractometer (CuK $\alpha$  radiation, 40 kV and 30 mA, with step of 0.0170 ° and accumulation of 200 seconds) and the data analyzed to obtain the lattice parameter, the crystallite size and composition of each phase identified.

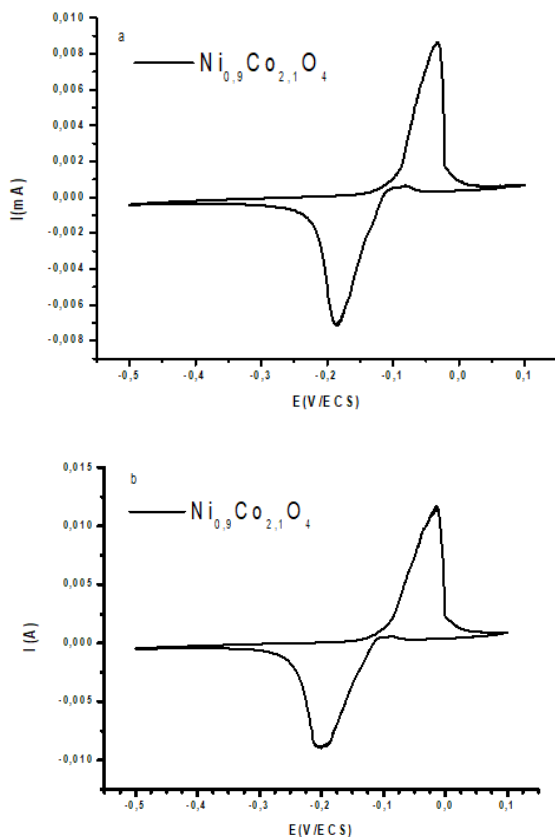


Fig.1. CV curves of Ni<sub>0.9</sub>Co<sub>2.1</sub>O<sub>4</sub> electrode at scan rates of 10 mV/s (a) and 20 mV/s (b)

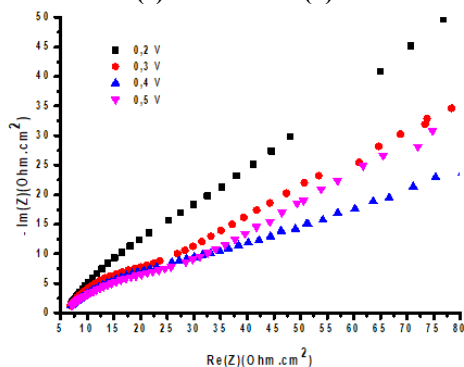


Fig.2. Nyquist plots for Ni<sub>0.9</sub>Co<sub>2.1</sub>O<sub>4</sub> oxide electrode at 0.2, 0.3, 0.4 and 0.5 V in 3 M KOH.

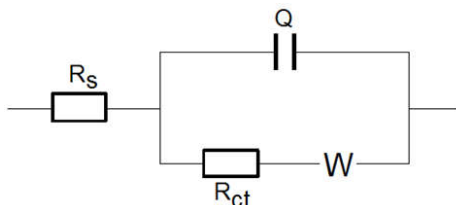


Fig. 3. Equivalent circuit modelling the impedance diagrams of Ni<sub>0.9</sub>Co<sub>2.1</sub>O<sub>4</sub> oxide electrode.

The specific surface area of the samples was determined using physical nitrogen adsorption isotherms and Brunauer Emmett and Teller (BET) theory using a Micrometrics Gemini apparatus with nitrogen gas as absorbent and liquid nitrogen as sample coolant (to ensure temperature stability). Cyclic voltammetry (CV), electrochemical impedance spectroscopy (EIS) and chronopotentiometry (CP) measurements were performed using a glass three-electrode cell layout at room temperature in KOH 3M aqueous solution as the electrolyte on a Potentiostat/Galvanostat Fra 2  $\mu$ Autolab Type III.

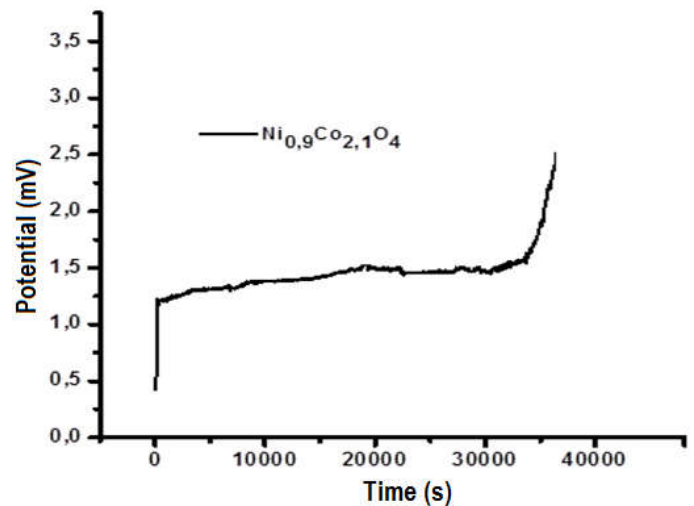


Fig.4. Chronopotentiometry curve of Ni<sub>0.9</sub>Co<sub>2.1</sub>O<sub>4</sub> electrode in 3 M KOH with a constant current density of 5 mA.cm<sup>-2</sup>

The preparation of the working electrode is detailed in our previous work (Mamadou Guèye, 2017).

## RESULTS AND DISCUSSION

By X-ray diffraction (XRD) characterization, we have already showed that obtained Ni<sub>0.9</sub>Co<sub>2.1</sub>O<sub>4</sub> powder prepared by sol-gel (propionic acid) method is in a crystallized phase with a face-centered cubic lattice and spinel structure (Mamadou Guèye, 2016). The cubic cell parameter,  $a$ , value was found to be 8.102 Å (Mamadou Guèye, 2016). The average size of crystallites ( $\tau_{\text{crystallite}}$ ) was calculated using the Scherrer equation. The grain size of the powder was evaluated by taking the average of the sizes corresponding to all peaks. The value obtained from XRD analyses is 49.57 nm. H. Nguyen-Cong *et al* (Nguyen-Cong, 2003) obtained with mixed oxides spinel type Ni<sub>x</sub>Co<sub>3-x</sub>O<sub>4</sub> prepared by the thermal decomposition of nitrate salts method and considering the full width at half maximum (FWHM) of the peak 311, a crystallite size of 35 nm in both cases where  $x = 0.3$  and 1. M. Mechouet *et al* (10) synthesized oxide powders of chemical composition Ni<sub>0.3</sub>Co<sub>2.7</sub>O<sub>4</sub> by the sol-gel method using two chelating agents (oxalic and citric acids) and two calcination temperatures (300 °C and 350 °C) and obtained average crystallite sizes of 16 and 25 nm with oxalic acid at 300 °C and 350 °C respectively, 13 and 20 nm with citric acid at 300 °C and 350 °C respectively.

Physical nitrogen adsorption isotherms was used to obtain the information on the specific surface area. Based on the nitrogen adsorption/desorption, Ni<sub>0.9</sub>Co<sub>2.1</sub>O<sub>4</sub> oxide particles exhibited a BET surface area of 16.82 m<sup>2</sup>/g. Similar specific surface values have been found in the literature. Huang Z-D *et al* (Huang *et al.*, 2016) found a specific surface value of 16.45 and 15.75 m<sup>2</sup>/g for NiCo<sub>2</sub>O<sub>4</sub> microspheres when calcined at 450 °C and 500 °C respectively. Bahaa M. Abu-Zied *et al.* (2014) reported a specific surface area value of 16.42 m<sup>2</sup>/g for  $x = 0$  with catalysts of the formula Ni<sub>x</sub>Co<sub>1-x</sub>Co<sub>2</sub>O<sub>4</sub> calcined at 500 °C. Other authors (Naveen, 2015), obtained the value of 19.25 m<sup>2</sup>/g with NiCo<sub>2</sub>O<sub>4</sub> nickel cobaltite powders. The electrochemical performance of spinel oxides Ni<sub>0.9</sub>Co<sub>2.1</sub>O<sub>4</sub> as oxygen electrocatalyst of reactions has been studied by cyclic voltammetry (CV) in a three electrode system with 3 M KOH aqueous electrolyte. Fig. 1 presents CV curves of Ni<sub>0.9</sub>Co<sub>2.1</sub>O<sub>4</sub> electrode material at sweep rates of 10 mV/s (Fig.1a) and 20 mV/s (Fig.1b) in a potential window ranging from -0.5 to 0.1

V. The CV shapes, clearly, reveal a pair of well-defined redox peaks, which is distinct from the ideal rectangular shapes typical of the electric double-layer capacity. And these peaks mainly indicate that the reaction mechanism in the electrode material is a faradic process. The anode and cathode peaks are around 0.013 V and -0.203 V, respectively and are associated with reversible reactions at the electrode surface of  $\text{Ni}^{3+}/\text{Ni}^{2+}$  and  $\text{Co}^{3+}/\text{Co}^{2+}$  pairs (An, 2014; Huang, 2013; Jiang, 2012; Wei, 2010; Yuan, 2012). Since nickel and cobalt ions undergo oxidation and reduction at neighboring potentials, it is difficult to separate the peaks corresponding to these ions in the cyclic voltammetry curve. Naveem *et al.* (2015) associated the oxidation peak in the voltammogram of a  $\text{NiCo}_2\text{O}_4$ -rGO oxide electrode in a 1 M KOH electrolytic solution at a scanning rate of 25 mV/s with transitions of nickel ions ( $\text{Ni}^{2+} \leftrightarrow \text{Ni}^{3+}$ ) and cobalt ions ( $\text{Co}^{2+} \leftrightarrow \text{Co}^{3+}$  and  $\text{Co}^{3+} \leftrightarrow \text{Co}^{4+}$ ). Gong *et al.* (20) and other researchers (Li, 2010; Chen, 2012) attributed the observed pair of redox peaks in the cyclic voltammetry curve of  $\text{NiCo}_2\text{O}_4$  nanofiber-based electrode to reversible reactions of  $\text{Co}^{4+}/\text{Co}^{3+}$  and  $\text{Ni}^{3+}/\text{Ni}^{2+}$  associated with  $\text{OH}^-$  ions. In a previous work (Mamadou Guèye, 2016), we have shown by XPS analysis that few  $\text{Co}^{2+}$  cations occupy the octahedral sites of  $\text{Ni}_{0.9}\text{Co}_{2.1}\text{O}_4$  spinel lattice and that the majority of cobalt found in the octahedral sites are  $\text{Co}^{3+}$ .

In the other hand, the majority of nickel ions found at the oxide surface are  $\text{Ni}^{2+}$  in octahedral sites. Combination of these results and those of CV characterization suggests that we obtained a mixed spinel structure. Moreover, EIS analysis have been carried out on the  $\text{Ni}_{0.9}\text{Co}_{2.1}\text{O}_4$  oxide electrode at potentials 0.2, 0.3, 0.4 and 0.5 V in 3 M KOH in order to gain an insight into the behavior of the material during oxygen reduction reaction. The impedance measurements were made in the form of Nyquist diagrams at frequencies ranging from 10 kHz to 100 mHz. As it can be seen in Fig.2. All the curves show a similar shape, consisting of a slightly flattened semicircle in the high frequency region and a straight line in the low frequency region. The semicircle is characteristic of a charge transfer and the linear part, with a slope close to  $45^\circ$  with respect to the real axis, is attributed to the diffusion phenomenon of  $\text{OH}^-$  ions from the electrolyte within the electrode (Ezeigwe, 2017). The diameter of the semicircle corresponds to the charge transfer resistance ( $R_{ct}$ ) of the electrode/electrolyte interface (Guèye, 2017; Ma, 2015; Umeshbabu, 2016; Zhu, 2015; Liang, 2012). The intersection, at high-frequency region of the impedance curve with the real axis, corresponds to the resistance of the mass of the electrochemical system ( $R_s$ ) (the resistance of the electrolyte, the intrinsic resistance of the material and the resistance at the active interface electrode material/current collector) (Umeshbabu *et al.*, 2016; Lu *et al.*, 2014; Umeshbabu *et al.*, 2014). The  $R_s$  values are the same for all the electrodes (Fig. 2) because the substrate and electrolyte are the same for all potentials. The inclined portion of the curve in the low frequency range is assigned to the Warburg impedance ( $Z_w$ ), which is induced by the diffusion/transport of electrolyte ions through the pores of the active material during redox reactions. The inclination of the linear part in the low frequency region close to the vertical reflects a capacitive behavior of the electrode (Umeshbabu *et al.*, 2016; Zhu, 2012; Stoller, 2008). As can be seen in Fig. 2, the diameter of the semicircle increases with the potential, corresponding to an increase in the value of the charge transfer resistance  $R_{ct}$ . Therefore, the electrical conductivity and catalysis for oxygen reactions decrease when the potential increases (Ma, 2015).

The linear part of the impedance curve moves further and further away from the ideal as the potential increases. Indeed, its slope gradually decreases with increasing potential, which shows that diffusion resistance increases with potential (Yang, 2014). These results show that an increase in the polarization potential is not favorable to an improvement in the electrochemical properties of the electrode. The equivalent circuit proposed to match most closely the impedance diagrams is in form of  $R_1(Q(R_2W))$  (Fig. 3), where  $R_1$ ,  $R_2$ ,  $Q$  and  $W$  represent solution resistance ( $R_s$ ), charge transfer resistance ( $R_{ct}$ ), pseudo-capacity ( $Q$ ) and Warburg impedance ( $W$ ), respectively. The stability of the  $\text{Ni}_{0.9}\text{Co}_{2.1}\text{O}_4$  oxide electrode which is also important for its practical application was tested in 3 M KOH aqueous solution by chronopotentiometry. It is measured by the time during which the potential to deliver the imposed current remains constant. As displayed in Fig. 4, the potential reached to deliver a current density of  $5 \text{ m A cm}^{-2}$  is 1.2 mV. The potential then stabilizes around this value during the 9 hours electrochemical transformations, with very small voltage fluctuations ( $< 0.5 \text{ mV}$ ), and the electrode is stable during the overall 9 h period. This indicate that the  $\text{Ni}_{0.9}\text{Co}_{2.1}\text{O}_4$  electrode as a good stability for the ORR in alkaline aqueous solution.

## Conclusion

$\text{Ni}_{0.9}\text{Co}_{2.1}\text{O}_4$  mixed valence was synthesized by sol-gel technic via propionic acid. The spinel oxide crystallized in a cubic centered faces phase with a cell parameter and an average crystallite size of 8.102 Å and 49.57 nm, respectively. The as-prepared Ni-Co mixed oxide offer a specific surface area of  $16.82 \text{ m}^2/\text{g}$  determined by BET method. The cyclic voltammetry study showed high electrical reactivity and rapid activation due to high electrode conductivity. No significant change in the voltammograms shape occurred when the scanning rate varied. The redox peaks remained symmetrical, indicating good electrochemical reversibility of the electrode. By EIS characterization, the evolution of the different parameters of the equivalent circuit as a function of the polarization potential of the interface allows us to conclude that increasing polarization potential do not favor the improvement of the electrochemical properties of the electrode. Chronopotentiometry shows that the potential remained almost constant throughout the electrochemical transformations at the electrode/electrolyte interface indicating a good electrical stability of the electrode in alkaline solution. These results show that  $\text{Ni}_{0.9}\text{Co}_{2.1}\text{O}_4$  type spinel mixed oxide powders are a promising high performance electrode for oxygen reduction reaction in alkaline media.

## REFERENCES

- Abu-Zied B. M., Soliman S. A., Abdellah S. E. 2014. *Chin. J. Catal.*, 35 1105-1112.
- An C., Wang Y., Huang Y., Xu Y., Xu C., Jiao L., Yuan H. 2014. *Nano Energy* 10 125-134.
- Boggio R., Carugati A. and Trasatti S. 1987. *J. Appl. Electrochem.*, 17 828.
- Chen X., Cheng J. P., Sou Q. L., Liu F., Zhang X. B. 2012. *Cryst. Eng. Comm.* 14 1271-1276.
- de Chialvo M.R.G. and Chialvo A.C. 1993. *Electrochim. Acta* 38 2247.
- Ezeigwe E. R., Khiew P. S., Siong C. W., Tan M. T. T. 2017. *J. Alloys Compd.* 693 1133-1142.

- Gong X., Cheng J. P., Liu F., Zhang L., Zhang X. 2014. *J. Power Sources* 267 610-616.
- Guèye M., Mandiamy P. C. H., Guène M., and Diagne A. 2017. *A., Int. J. Adv. Res.*, 5 (8) 816-823.
- Hu C.C., Lee Y.-S., Wen T.C. 1997. *Mat. Chem. Phys.* 48 246-254.
- Huang L., Chen D., Ding Y., Feng S., Wang Z. L., Liu M. 2013. *Nano Lett.*, 13 3135.
- Huang Z.D., Zhang K., Zhang T.-T., Yang X.-S., Liu R.Q., Li Y., Lin X.-J., Feng X.M., Ma Y.-, Huang W. 2016. *Energy Storage Materials* 3 36–44.
- Jiang H., Ma J., Li C. Z. 2012. *Chem. Commun.* 48 4465.
- Li Y. G., Hasin P., Wu Y. Y. 2010. *Adv. Mater.* 22 1926-1929.
- Liang K., Tang X., Hu W. 2012. *J. Mater. Chem.* 22 11062-11067.
- Lu Y., Yan H., Zhang D., Lin J., Xue Y., Li J., Luo Y., Tang C., *J. Solid State Electrochem.* 18 3143–3152.
- Ma L., Shen X., Zhou H., Ji Z., Chen K., Zhu G. 2015. *Chem. Eng. J.* 262 980–988.
- Mamadou Guèye, Makhtar Guène, 2016. *J. Soc. Ouest-Afr. Chim* 041 ; 35-40.
- Mamadou Guèye, Papa Charles Harris Mandiamy, 2017. Makhtar Guène and Abdou Aziz Diagne, *Int. J. Adv. Res.* 5(8) 816-823.
- Mechouet M., Idiri N., Belkessam C., Kadri A., Benbrahim N. 2016. *Processing and Application of Ceramics* 10 (2) 107–115.
- Naveen A. N., Selladurai S. 2015. *Electrochim. Acta* 173 290–301.
- Naveen A. N., Selladurai S. 2015. *Electrochimica Acta.*, 173 290–301.
- Nguyen-Cong H., de la Garza Guadarrama V., Gautier J.L., Chartier P. 2003. *Electrochim. Acta*, 48 (17) 2389–2395.
- Rios E., Gautier J.L., Poillierat G., Chartier P. 1998. *Electrochim. Acta* 44 1491-1497.
- Stoller M. D., Park S., Zhu Y., An J., Ruoff R. S. 2008. *Nano Lett.* 8 3498-3502.
- Trasatti S., J. 1994. Lipkowski and Ph. Ross (Eds.), *Electrochemistry of Novel Materials*, VCH Publishers III 207.
- Umeshbabu E., Rajeshkhanna G., Rao G. R. 2014. *Int. J. Hydrog. Energy.*, 39 15627–15638.
- Umeshbabu E., Rajeshkhanna G., Rao G. R. 2016. *J. Solid State Electrochem.* 20(7) 1837-1844.
- Veggetti E., Kodintsev I.M. and Trasatti S. 1992. *J. Electroanal. Chem.* 339 255.
- Wei T. Y., Chen C. H., Chien H. C., Lu S. Y., Hu C. C. 2010. *Adv. Mater.* 22 347.
- Yang Q., Lu Z., Li T., Sunn X., Liu J. 2014. *Nano Energy.*, 7 170–178.
- Yuan C., Li J., Hou L., Zhang X., Shen L., Lou X. W. D., 2012. *Adv. Funct. Mater.* 22 4592.
- Zhu Y., Wang J., Wu Z., Jing M., Hou H., Jia X., Ji X. 2015. *J. Power Sources.*, 287 307-315.

\*\*\*\*\*